



Alumina–silica glass–ceramic sealants for tubular solid oxide fuel cells

N. S. Saetova¹ , D. A. Krainova^{1,2} , A. V. Kuzmin^{1,2,*} , A. A. Raskovalov¹ ,
S. T. Zharkina^{1,2} , N. M. Porotnikova^{1,2} , A. S. Farlenkov^{1,2} , N. I. Moskalenko¹ ,
M. V. Ananyev^{1,2} , M. V. Dyadenko³ , and S. Ghosh⁴

¹Institute of High-Temperature Electrochemistry, Ural Branch, Russian Academy of Sciences, Yekaterinburg, Russia

²Yeltsin Ural Federal University, Yekaterinburg, Russia

³Belarusian State University of Technology, Minsk, Belarus

⁴Indian Institute of Engineering Science & Technology, Howrah, West Bengal 711103, India

Received: 29 August 2018

Accepted: 21 November 2018

Published online:

3 December 2018

© Springer Science+Business
Media, LLC, part of Springer
Nature 2018

ABSTRACT

In this work, we synthesized the glasses of the $\text{SiO}_2\text{--Al}_2\text{O}_3\text{--CaO--Na}_2\text{O--MgO--K}_2\text{O--B}_2\text{O}_3\text{--Y}_2\text{O}_3$ system and investigated their thermal properties under changes in the ratios between the components in both modifying (MgO/CaO) and glass-forming ($\text{SiO}_2/\text{B}_2\text{O}_3$) oxides. In addition, the effects of crystallization on both the properties of sealants and their behaviour at the boundary with ceramic yttria-stabilized zirconia (YSZ) electrolyte have been studied. X-ray diffraction analysis was used to determine the phase composition of the glasses both after quenching, dilatometric measurements and sealing of the glasses with the YSZ ceramic support. The thermal expansion coefficients (CTEs) found for the glasses and glass–ceramics are shown to be in good agreement with those of other cell components. The sealing temperatures of these materials are found to be lower than the operating temperature limit of the interconnector alloy. It is shown that Mg-rich glasses exhibit higher resistance to interaction with Cr compared to other compositions under study. The scanning electron microscopy and energy dispersive spectroscopy studies have confirmed the formation of gas-tight connections by the sealants under investigation. The glass demonstrating the highest stability in contact with the Crofer22APU alloy has been tested as a sealant for a tubular cell. This material is established to ensure a tight connection without cracks during operation at 850 °C for 250 h. The materials are thus found to be promising candidates for use as sealants for solid oxide fuel cells (SOFCs).

Address correspondence to E-mail: a.v.kuzmin@yandex.ru

Introduction

One of the most important issues that should be addressed when creating stable solid oxide fuel cells (SOFCs) involves the development of sealants capable of ensuring a gas-tight connection between SOFC elements [1]. Numerous requirements are imposed upon sealants for SOFCs. These include their chemical stability in both oxidizing and reducing atmospheres, appropriate linear thermal expansion coefficients (CTEs), capability of prolonged operation at high temperatures (800–1000 °C) without degradation, high electrical resistance for avoiding electrical short circuits, etc. [2, 3]. Fulfilling all these requirements, glasses and glass–ceramics are considered to be promising candidates as SOFC sealants [4]. An additional advantage of glass sealants consists in their viscous-flow state at the high temperatures of SOFC operation, which significantly reduces mechanical stresses between SOFC components [5, 6]. However, glasses can undergo partial or complete crystallization during SOFC operation, which may lead to a increase in the glass viscosity and a subsequent cracking of the sealant, thus making the entire SOFC structure depressurized [7–10]. Another disadvantage of glasses is the possibility of chemical interactions between them and the interconnector materials [11]. Despite these drawbacks, high-temperature silicate glasses have been successfully applied as sealing materials, sustaining SOFC operating conditions for 1000 h without a significant degradation in their functional properties [12–14].

A series of works have been carried out by F. Smeacetto et al. to study the properties of SiO_2 – Al_2O_3 – CaO – Na_2O glass materials as sealants for SOFCs [15–28]. The investigation of the stability of SiO_2 – Al_2O_3 – CaO – Na_2O glass sealants in contact with stainless steel interconnectors (made of pre-oxidized Crofer22APU or AISI 430) and yttria-stabilized zirconia (YSZ) ceramic has been reported in [15]. It was shown that no chemical interactions occur at the boundaries between ceramic YSZ/glass sealant/alloy during the periods of 400 h and 200 h in the air and H_2 – $3\text{H}_2\text{O}$ atmospheres, respectively. The behaviour of SiO_2 – Al_2O_3 – CaO – Na_2O glass sealants under different conditions was also investigated using a Crofer22APU/glass/YSZ electrolyte unit cell [18–22]. The degradation of the cell materials did not occur under prolonged operation at 800 °C and thermal cycling across the temperature range of 25–800 °C in

the H_2 – $3\text{H}_2\text{O}$ atmosphere [18]. Similar experiments in the air atmosphere have shown the diffusion of Cr and Mn from the alloy to the sealant to occur, leading to the formation of a thin layer of the $\text{Mn}_3\text{Cr}_2\text{Si}_3\text{O}_{12}$ phase on the Crofer22APU/glass boundary [19]. Furthermore, on the surface of the Crofer22APU alloy, Al_2O_3 formed as a result of the diffusion and oxidation of aluminium, which is a constituent of the alloy composition. When testing the cell under conditions close to the operating conditions of SOFC ($T = 820$ °C, $p_{\text{H}_2} = 0.959$; $p_{\text{H}_2\text{O}} = 0.041$, $p_{\text{O}_2} = 0.21$, $p = 1$ atm), a decrease in voltage was observed after continuous operation for 460 h [19]. This was shown to result from the cathode material degradation caused by chromium.

A comparative study of two stacks consisting of several elements and operating at 800 °C in the dry air atmosphere was presented in [21]. In the first case, no protective coating was applied on the interconnector, which led to the degradation of the characteristics after operating the cell for 250 h. The reason for such degradation was the diffusion of chromium from the Crofer22APU alloy into the cathode material. In the second case, a $\text{Mn}_{1.5}\text{Co}_{1.5}\text{O}_4$ -coated interconnector was used, which permitted an increase in the operating time of the element of up to 350 h, without degradation of its materials. In another study, the glass of the 53.3SiO_2 – $12\text{Al}_2\text{O}_3$ – 22.5CaO – $12.2\text{Na}_2\text{O}$ composition was selected to perform thermal cycling (the maximal temperature of 800 °C) for 3000 h in the air atmosphere with different heating rates [22]. The experiment proved that the material degradation is insignificant at the glass sealant/YSZ ceramic boundary. However, the Crofer22APU alloy was demonstrated to oxidize under the specified operating conditions, which lead to the diffusion of chromium and manganese into the glass near the glass/Crofer22APU boundary. In addition, the authors noted an unusual feature of this sealant, which differs this material from similar compositions. During operation, the $\text{CaAl}_2\text{Si}_2\text{O}_8$ phase formed near voids in the sealant bulk. The authors explained the existence of this phase by the diffusion of calcium from the interphase boundaries to the bulk glass. Despite the above-mentioned disadvantages, this glass provided a good adhesion to Crofer22APU and YSZ ceramic and showed no cracks during the entire operating time [22].

The stability of a 54.39SiO_2 – $11.26\text{Al}_2\text{O}_3$ – 9.02CaO – $13.78\text{Na}_2\text{O}$ – 8.37MgO – $1.67\text{K}_2\text{O}$ – $0.9\text{B}_2\text{O}_3$ – $0.61\text{Y}_2\text{O}_3$

Table 1 Nominal chemical composition and results of AES and XFS analysis of the studied glasses (in wt.%)

	SiO ₂	Al ₂ O ₃	CaO	Na ₂ O	MgO	K ₂ O	B ₂ O ₃	Y ₂ O ₃
1 nominal	54.39	11.26	9.02	13.78	8.37	1.67	0.90	0.61
1 AES	52.66	12.11	10.40	15.55	5.20	1.71	0.80	1.12
1 XFS	51.40	12.36	9.31	14.47	9.15	1.54	0.89	0.56
2 nominal	54.39	11.26	5.02	13.78	12.37	1.67	0.90	0.61
2 AES	55.30	10.73	5.69	13.92	10.79	1.56	0.94	0.64
2 XFS	53.72	12.03	5.10	14.48	11.51	1.58	0.76	0.51
3 nominal	56.39	11.26	9.02	11.78	8.37	1.67	0.90	0.61
3 AES	54.86	11.17	10.18	12.80	7.57	1.68	0.89	0.66
3 XFS	55.30	11.19	9.97	12.45	7.34	1.70	0.75	0.53
4 nominal	53.29	11.26	9.02	13.78	8.37	1.67	2.00	0.61
4 AES	52.51	11.61	9.37	13.75	7.85	1.56	2.10	0.60
4 XFS	51.54	12.92	9.59	13.69	7.93	1.64	1.12	0.61
5 nominal	51.29	11.26	9.02	13.78	8.37	1.67	4.00	0.61
5 AES	51.81	11.21	8.89	14.60	7.47	1.60	3.59	0.61
5 XFS	51.50	12.53	9.81	13.84	8.00	1.58	1.28	0.62
6 nominal	49.29	11.26	9.02	13.78	8.37	1.67	6.00	0.61
6 AES	46.67	12.32	9.17	15.30	7.89	1.65	6.20	0.64
6 XFS	53.08	13.29	8.43	13.62	7.19	1.57	1.58	0.58

glass sealant in contact with the Crofer22APU material covered by Mn_{1.5}Co_{1.5}O₄ and YSZ ceramic was investigated in [2]. According to the data obtained, this glass is a promising material for SOFC application, due to its suitable thermal coefficient of linear expansion (8.5·10⁻⁶ and 10.9·10⁻⁶ K⁻¹ for original glass and glass–ceramic, respectively) and the absence of reaction with the interconnector material after 500 h of cycling across the 25–850 °C temperature range. It should be noted that rare pores are present in the bulk of this glass, which can lead to the degradation of the material during a longer operating time. In [29], the effect of cerium oxide at various concentrations on SiO₂–Al₂O₃–CaO–Na₂O–MgO–K₂O–B₂O₃–Y₂O₃ glasses was investigated. It was established that an increase in CeO₂ concentration results in an increase in the CTE of the amorphous samples and a decrease in the CTE of the glass–ceramic (GC) ones. A difference between the CTEs of the amorphous and glass–ceramic materials was negligible. The glasses obtained in work [29] provide a tight connection between the cell elements at temperatures below the maximum operating temperature of the interconnector material (CroferAPU alloy).

The composition of the sealant is normally selected depending on both the materials of the elements that are to be sealed and the entire SOFC construction. The vast majority of studies devoted to sealing materials deal with the development of the planar

design SOFCs, with the tubular design attracting significantly less attention. At the same time, the design of tubular SOFCs requires a much thinner sealing layer, thus imposing stricter requirements on the properties of sealing materials.

This study is aimed at decreasing the linear thermal expansion coefficient of SiO₂–Al₂O₃–CaO–Na₂O–MgO–K₂O–B₂O₃–Y₂O₃ glasses by varying the ratios between the components in both modifying (MgO/CaO) and glass-forming (SiO₂/B₂O₃) oxides. In addition, we investigate the effect of crystallization on both the properties of sealants and the behaviour of the sealant/ceramic YSZ electrolyte boundary.

Experimental

CaCO₃, Na₂CO₃ (chemically pure grade), SiO₂ (hydrous), K₂CO₃, B₂O₃, MgO, Al₂O₃ (ultrapure grade) and Y₂O₃ (chemically pure grade) were used as the initial reagents. All components of the batch were taken in a stoichiometric ratio according to Table 1. A roller mill was used to homogenize the batch for the preparation of glasses. The mixing was carried out in a glass vessel at a room temperature for 30 min. Preliminary annealing was performed at a temperature of 600 °C, followed by cooling to a room temperature and pressing of batch tablets. The batch tablets were heated in an alumina crucible up to 1480 °C with the dwelling time of 15 min.

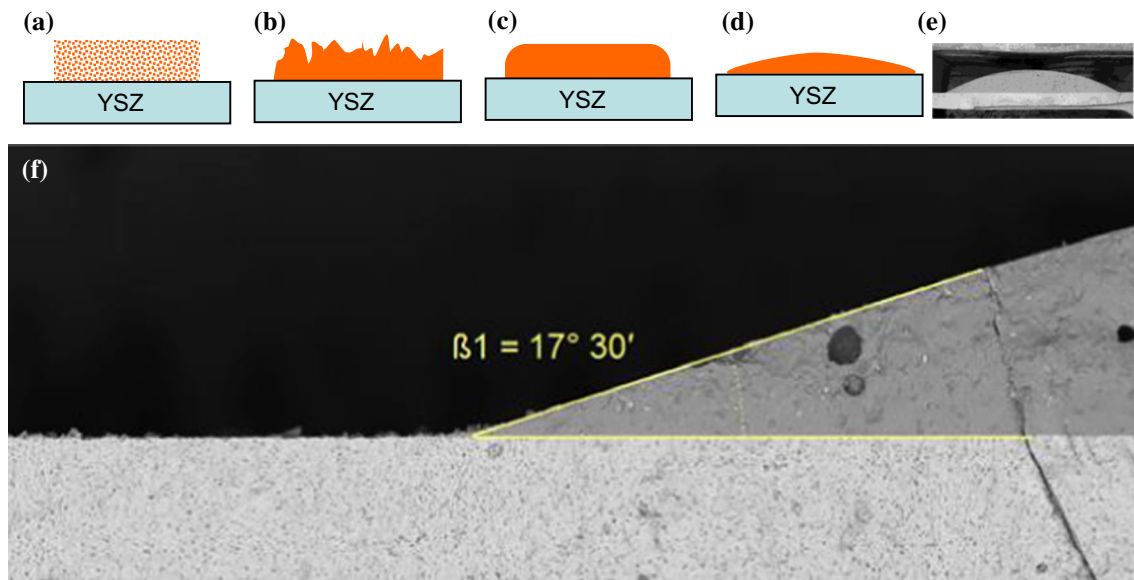


Figure 1 Evolution of the glass sample on YSZ substrate with temperature: **a** a powdered sample with a polymeric binder, **b** after the polymer combustion, **c** beginning of a drop formation, **d** a drop

in the case of good adhesion, **e** an example of real glass with good adhesion to YSZ and **f** the contact angle SEM images in BSE mode.

Subsequently, the melt was cast into a glassy-carbon mould. As a result, transparent glass was obtained. The glass was annealed in a muffle furnace at a temperature of 560 °C for 30 min, followed by slow cooling to a room temperature. In order to obtain glass-ceramic (GC) samples, glass powder (size particle < 45 μm) was pressed and heat-treated at 950 °C in a tubular furnace.

The phase composition of the as-obtained glass and glass-ceramic samples was determined using a D/MAX-2200VL/PC X-ray diffractometer (Rigaku, Japan) with $\text{CuK}\alpha$ radiation ($\lambda = 1.5418 \text{ \AA}$), a scanning rate of 2°/min and a range of 2θ from 10° to 65°.

For chemical analysis, the glasses were ground to a powder. The powder (0.1 g) was then dissolved in a mixture of hydrochloric, nitric and hydrofluoric acids in a microwave sample preparation system (Multiwave, Anton Paar) following the recommendations provided in the manual. The solutions of the samples were diluted to the volume of 100 ml by deionized water. A spectrometer Optima 4300 DV (Perkin Elmer, USA) with inductively coupled plasma was calibrated using state reference materials (solutions of Si, Na, Al, Mg, Ca, K, B and Y compounds). The measurements were performed with an accuracy of 2–3%. In addition, a Lab Center XRF-1800 (Shimadzu, Japan) X-ray fluorescence wavelength-dispersive

spectrometer of sequential action was used to confirm the chemical composition of the samples.

The characteristic temperatures of the glasses under study were determined by differential scanning calorimetry (DSC) coupled with thermogravimetry using a STA 449 F1 Jupiter thermal analysis device (NETZSCH, Germany). The measurements were carried out in a platinum crucible in an argon atmosphere (blowdown rate—20 ml/min) with a heating rate of 10 K/min across the 50–950 °C temperature range. DSC spectrum analysis and peak separation were carried out using the NETZSCH Proteus software. The accuracy of the measurements was $\pm 1 \text{ }^\circ\text{C}$.

In order to determine the values of thermal linear expansion coefficient (CTE), the bar-shaped samples ($5 \times 5 \times 10 \text{ mm}$) were produced. The glass samples were cut out from the bulk glass, while the glass-ceramic samples were pressed from the powdered glass. The measurements were carried out using a dilatometer Tesatronic TT-80 (TESA, Switzerland) with a measuring probe TESAGT 21HP ($\pm 200 \text{ }\mu\text{m}$ measurement range, $0.01 \text{ }\mu\text{m}$ sensitivity) in the range of temperatures 50–600 °C.

In order to determine sealing temperatures, the glass powder was mixed with a polymeric binder and applied to a YSZ ceramic substrate (Fig. 1a). Subsequently, the as-obtained “sandwich” was

placed into a furnace and treated as follows: heated to a definite temperature—held for 10 min—cooled. During heating, the organic binder is burning out at a temperature of ~ 400 °C, with the surface of the sealing glass becoming heterogeneous (Fig. 1b). During further heating, the glass powder is undergoing compaction, forming a tight mass due to the transition of the glass into the viscous-flow state at temperatures higher than the glass transition temperature (Fig. 1c). Afterwards, the viscosity of the glass decreases, allowing it to spread over the surface of the substrate with the formation of a smooth drop. The value of the contact angle indicates the wettability of the glass: small contact angles ($< 90^\circ$) correspond to its high wettability (and good adhesion), while large contact angles ($> 90^\circ$) correspond to its low wettability [30]. The temperature, at which the glass produced a smooth homogeneous drop with a small contact angle (Fig. 1d) to YSZ, was considered to be its sealing temperature. Figure 1e, f shows a microphotograph of such a glass drop after the aforementioned treatment. For comparison, in works [27, 31] sealing temperatures were defined by a glass drop shape using a similar method.

The microstructure of the compositions under investigation was studied by scanning electron microscopy using a MIRA 3LMU (TESCAN, Czech Republic). SEM images in SE (secondary electrons) and BSE (back-scattered electrons) modes were obtained at a high voltage of 10 kV and beam intensity of 10. The high voltage of 20 kV and the beam

intensity of 15 were used for the EDX analysis. In order to obtain satisfactory SEM images, the samples were pre-treated by the epoxy impregnation technique under vacuum. The cross sections of the samples were obtained by a Struers Labopol polishing-grinding machine using a diamond suspension. In addition, the element distribution maps of the sealed “sandwiches” were obtained by means of the energy dispersive spectrometry (EDS) method.

Results and discussion

Characterization

According to the X-ray diffraction analysis (XRD) data, all glass samples exhibit an amorphous structure after melt casting (Fig. 2a). Table 1 shows the chemical composition of the glasses estimated by atomic emission spectroscopy (AES) and X-ray fluorescence spectroscopy (XFS). The results of the analyses are consistent with both each other and the nominal composition of the glasses. It should be noted that the XFS method underestimates B_2O_3 concentration, most likely due to a slight diffusion of X-rays by light elements.

Characteristic temperatures

The characteristic temperatures of the synthesized glasses were determined by DSC. According to the DSC curves (Fig. 3), both exothermic peaks in the

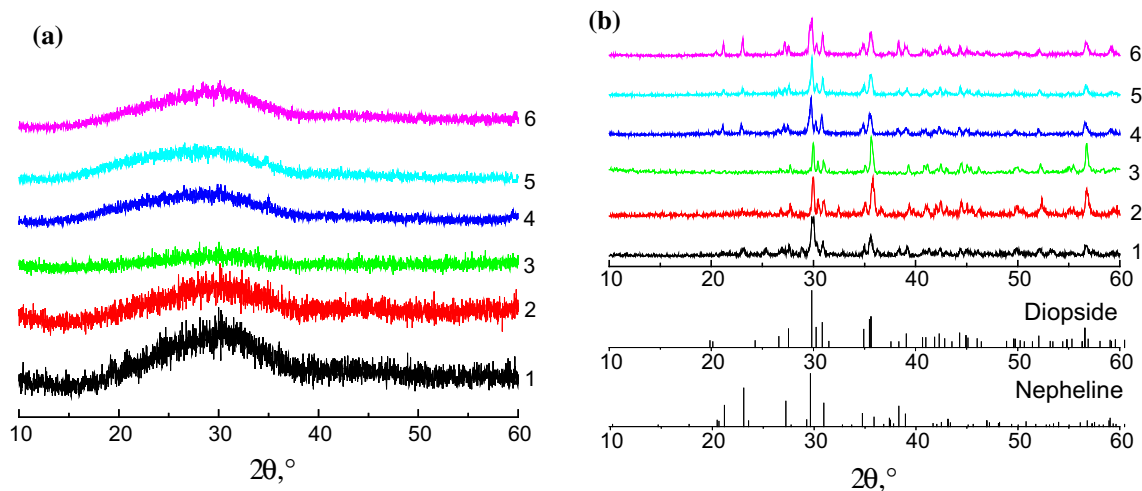


Figure 2 X-ray patterns of the obtained glasses of $SiO_2-Al_2O_3-CaO-Na_2O-MgO-K_2O-B_2O_3-Y_2O_3$ system (a), pressed powdered glass after annealing (b). The composition numbers

correspond to Table 1 (#2: CaO content is decreased, MgO—increased (CaO \rightarrow MgO); #3: $Na_2O \rightarrow SiO_2$; #4–6 $SiO_2 \rightarrow B_2O_3$).

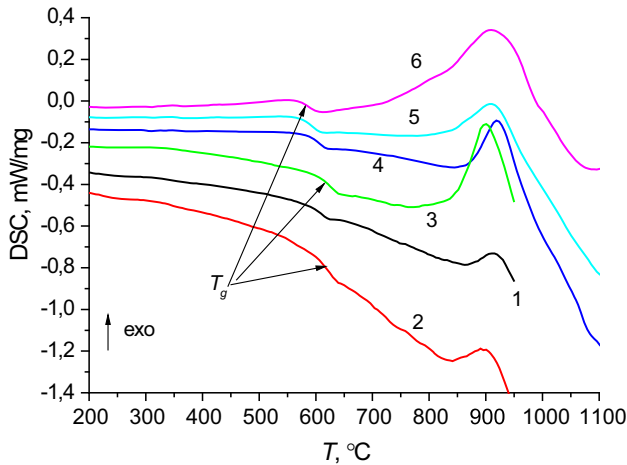


Figure 3 DSC curves of glasses SiO₂-Al₂O₃-CaO-Na₂O-MgO-K₂O-B₂O₃-Y₂O₃ system.

temperature range 750–950 °C corresponding to crystallization and bends corresponding to the glass transition temperature (T_g) were observed. The endothermic effect after the crystallization point corresponds to the melting of the system. The characteristic temperatures of the glasses are summarized in Table 2. It can be seen that an increase in the boron oxide content results in a decrease in T_g . It is common knowledge that boron oxide reduces the characteristic temperature of glasses due to its low melting temperature. In our experiments, changes in the characteristic temperatures of the glasses, which had occurred as a result of varying the ratios MgO/CaO and SiO₂/Na₂O, were similar. The glass transition (T_g) and crystallization (T_{c1} , T_{c2}) temperatures increase along with the growth of the MgO and SiO₂ content. It should be noted that the T_g determined by DSC is higher than that determined by dilatometry, which has been shown to be typical of different types of glasses [32, 33]. This difference might be explained by the different heating rates of these methods: 2 and 10°/min for dilatometry and DSC, respectively [34].

Table 2 Characteristic temperatures of the obtained glasses. The data are given with the accuracy of ± 1 °C

Composition	T_g , °C		T_c , °C		T_d , °C	
	DSC	Dilatometry	Onset (T_{c1})	Peak (T_{c2})	Glass	GC
1	602	545	862	914	855	884
2	608	550	838	893	882	866
3	615	540	852	890	878	876
4	602	570	870	919	874	867
5	590	570	834	910	864	845
6	587	565	838	909	842	810

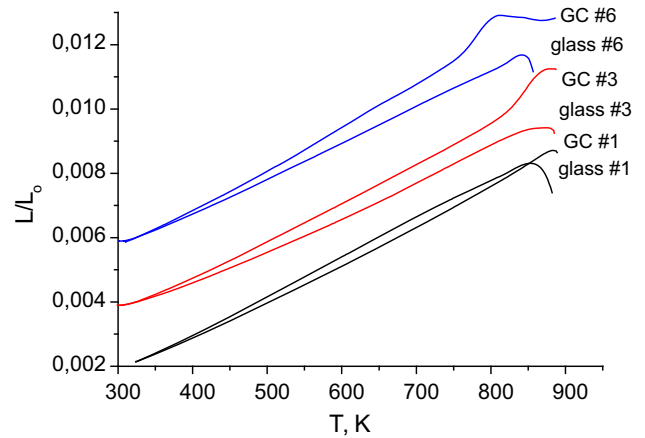


Figure 4 Dilatometric curves obtained from both bulk amorphous (glass) and powdered crystalline samples.

The deformation temperatures (T_d) were determined according to the dilatometry curves obtained for the glass and GC samples (Table 2). Glasses possess a higher softening point than the corresponding GCs; however, sample #1 has an invert tendency due to a higher quantity of the residual glass phase.

Coefficient of thermal expansion

CTE measurements were carried out on both amorphous original glasses and the corresponding glass-ceramics (GC) obtained by heat treatment at 950 °C. In the GC samples, crystalline phases are observed, including diopside (CaMgSi₂O₆) and nepheline (NaAlSi₃O₈) with the CTE of 16·10⁻⁶ K⁻¹ [35] (Fig. 2b). Dilatometric curves for some samples are shown in Fig. 4.

CTE is defined as the derivative of linear expansion with respect to temperature. Therefore, the dependence of the relative expansion (Y) on temperature can be presented as a function. Then, it becomes easy to obtain an equation for CTE by differentiating this function. A previous study [29] found that the

following function can suitably describe the experimental data within the 298–673 K temperature range:

$$\frac{\Delta l}{l_0} \equiv Y(T) = a + bT + cT^2 + \frac{d}{T}, \quad (1)$$

where a , b , c and d are empirical coefficients, and T is temperature. In this case, the CTE (α), being a derivative of function (1), is expressed as:

$$\alpha(T) = \frac{dY}{dT} = b + 2cT - \frac{d}{T^2}. \quad (2)$$

Equation (2) gives CTE as a function of temperature. The average value of α across a desired temperature range can be obtained by integrating Eq. (2) with normalization to the range:

$$\bar{\alpha} = \frac{1}{T_2 - T_1} \int_{T_1}^{T_2} \alpha(T) dT, \quad (3)$$

where T_1 and T_2 are the first and the last temperatures within this temperature range. Taking into account Eq. (2) and the chosen temperature range, Eq. (3) can be written as follows:

$$\bar{\alpha} = \frac{1}{673 - 298} \left(b(673 - 298) + c(673^2 - 298^2) + d \left(\frac{1}{673} - \frac{1}{298} \right) \right). \quad (4)$$

The obtained values of the average CTE for the synthesized glasses and glass ceramics are given in Table 3. It seems interesting to compare the obtained CTE values with those theoretically predicted. A method that can be used for such a theoretical prediction was proposed by Appen in [36]. Following this method, CTE is calculated as follows:

$$K = \frac{\sum n_i \bar{k}_i}{\sum n_i}, \quad (5)$$

where K is an estimated value of the property, \bar{k}_i is an approximate average value of this property, and n_i is the oxide content (mole fraction). The CTE increments (\bar{k}_i) were taken from [36] to be equal to 3.8, –3.0, 6.0, 13.0, 39.5 and 46.5 for SiO₂, Al₂O₃, MgO, CaO, Na₂O and K₂O, respectively. The approximate average values of CTE for B₂O₃ vary significantly during transition from one glass group to another. These values primarily depend on the ratio of a total molar

Table 3 Measured and calculated CTE values for glasses and GCs in the range 298–673 K

Composition	$a \cdot 10^3$	$b \cdot 10^6, K^{-1}$	$c \cdot 10^{10}, K^{-2}$	d, K	$\alpha_{298-673}, 10^{-6} K^{-1}$	$\alpha_A, 10^{-6} K^{-1}$
YSZ10	–				9.4	–
Crofer22APU	–				12.1	–
Glasses						
1	-3.75 ± 0.09	9.70 ± 0.20	21.20 ± 1.00	0.16 ± 0.01	10.9	9.8
2	-2.91 ± 0.07	7.10 ± 0.10	31.60 ± 0.80	0.08 ± 0.01	9.8	9.4
3	-2.92 ± 0.12	6.40 ± 0.20	39.70 ± 1.50	0.13 ± 0.02	9.6	9.1
4	-3.57 ± 0.08	9.30 ± 0.20	17.70 ± 1.00	0.11 ± 0.01	10.5	9.7
5	-5.65 ± 0.08	13.70 ± 0.20	-12.40 ± 1.00	0.43 ± 0.01	10.4	9.5
6	-6.45 ± 0.09	15.30 ± 0.2	-19.40 ± 1.10	0.55 ± 0.01	10.6	9.4
Glass–ceramics						
1	-8.97 ± 0.12	21.30 ± 0.20	52.60 ± 1.40	0.90 ± 0.02	11.7	–
2	-4.75 ± 0.07	11.60 ± 0.10	4.80 ± 0.20	0.30 ± 0.01	10.6	–
3	-6.61 ± 0.10	15.30 ± 0.20	13.50 ± 1.20	0.58 ± 0.02	11.1	–
4	-7.38 ± 0.14	17.00 ± 0.30	-20.20 ± 1.60	0.67 ± 0.02	11.7	–
5	-5.80 ± 0.10	14.10 ± 0.20	-2.90 ± 1.20	0.40 ± 0.01	11.8	–
6	-7.85 ± 0.29	17.60 ± 0.60	16.20 ± 1.70	0.75 ± 0.05	12.3	–

(α_A —CTE of glass, calculated by Appen method; $\alpha_{298-673}$ —CTE of YSZ, Crofer22APU, glasses and GCs obtained after the dilatometric curves treatment; a , b , c and d —empirical coefficients, obtained by fitting of experimental data by Eq. (1) in the range of 298–775 K). The calculated values are determined with accuracy of $\pm 0.2 \cdot 10^{-6} K^{-1}$. CTE of Crofer22APU alloy and YSZ10 ceramics was measured by us

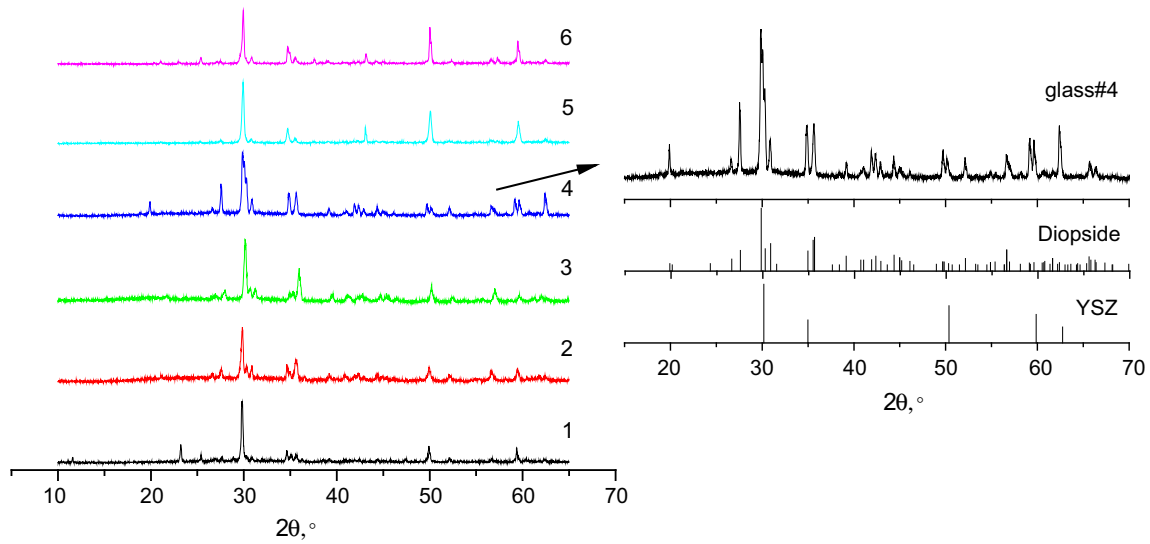


Figure 5 X-ray patterns of obtained glasses of the $\text{SiO}_2\text{--Al}_2\text{O}_3\text{--CaO--Na}_2\text{O--MgO--K}_2\text{O--B}_2\text{O}_3\text{--Y}_2\text{O}_3$ system on the YSZ substrate after the determination of the sealing temperature. The

composition numbers correspond to Table 1 (#2: CaO content is decreased, MgO—increased (CaO → MgO); #3: $\text{Na}_2\text{O} \rightarrow \text{SiO}_2$; #4-6 $\text{SiO}_2 \rightarrow \text{B}_2\text{O}_3$).

content of metal oxides to that of boron anhydride (ψ), given by [36]:

$$\psi_1 = \frac{N_{\text{Me}_2\text{O}} + N_{\text{MeO}} - N_{\text{Al}_2\text{O}_3}}{N_{\text{B}_2\text{O}_3}}, \quad (6)$$

According to formula (6), ψ is equal to 40.69 for glass #2. The average CTE of boron oxide was determined according to the calculated ψ value. In a similar manner, the CTE value was calculated for each glass using formula (5). According to [37], the accuracy of the calculated linear coefficient of thermal expansion varies within $\pm 0.2 \cdot 10^{-6} \text{ K}^{-1}$. The deviation of the CTE determination from the experimental data is given in Table 3. The obtained values are presented in Table 3. It can be seen from Table 3 that, except for composition #6, the following rule is satisfied: the higher the CTE value obtained by the Appen method, the higher the expansion coefficient found experimentally.

As can be seen from Table 3, the CTE values of the glass–ceramic samples are higher than those of original glasses. It can be explained by the higher CTE values of the crystalline phases. Apparently, the CTE of the obtained GCs depends on the ratio of the amorphous and crystalline phases formed during SOFC operation. Both the substitution of calcium oxide by magnesium oxide and the substitution of sodium oxide by silica lead to a sharp decrease in CTE values compared to the initial composition (#1)

taken from [2]. This effect is related to the difference between the ionic radii of the elements. It should be mentioned that the $\text{Na}_2\text{O}/\text{SiO}_2$ ratio has a greater impact on the CTE values of GC materials than the MgO/CaO ratio, since the radius of Si^{4+} is significantly smaller than that of Na^+ . The substitution of SiO_2 by B_2O_3 insignificantly affects the CTE values of glass materials, although increasing those of glass-crystalline materials. The CTEs of the glass-crystalline materials are in good agreement with the CTEs of both the interconnect material and YSZ ceramic electrolyte ($12.1 \cdot 10^{-6}$ and $9.4 \cdot 10^{-6} \text{ K}^{-1}$, respectively). It can therefore be concluded that these glasses can be applied as sealants for SOFC.

Microstructure

According to a change in the shape of a glass droplet (see Experimental), the sealing temperatures of glass samples #1–6 are found to be 1070, 1090, 1100, 1090, 1080 and 1070 °C, respectively. The XRD patterns of the glasses after sealing are presented in Fig. 5. It can be seen that no interaction occurs between the glass sealants and the YSZ ceramics support. The formed crystalline phases are similar to those shown in Fig. 2b. Overall, the sealing temperatures of these glass sealants do not exceed the maximum permissible temperature of the Crofer22APU heat-resistant alloy (1100 °C) and its analogues used as interconnector materials for SOFCs. Following the

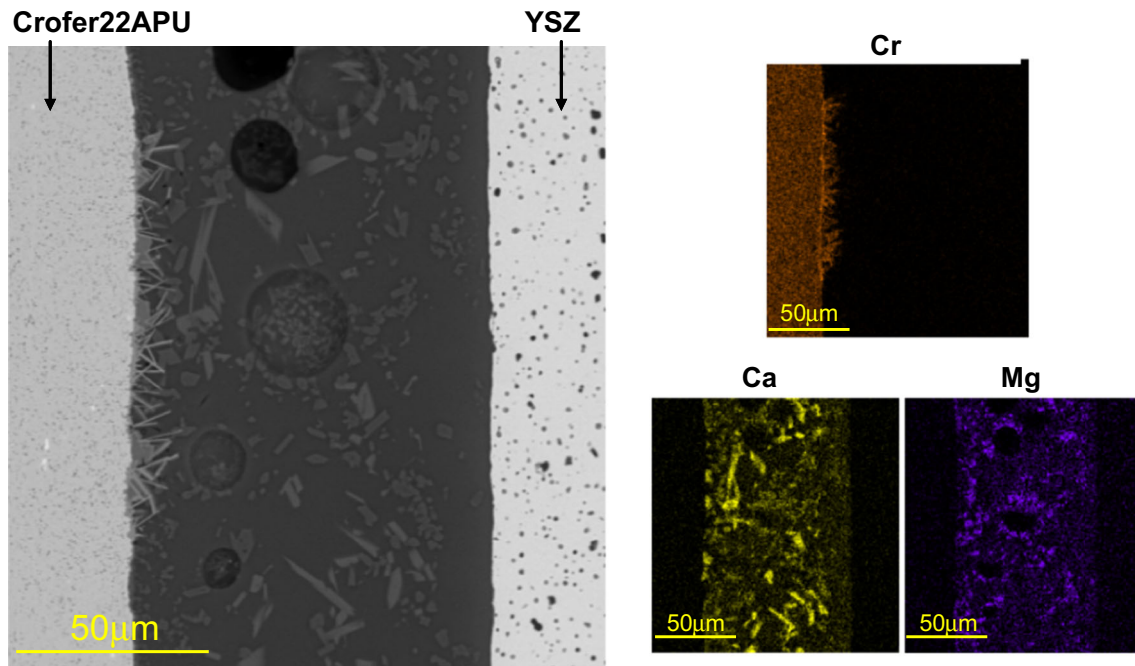


Figure 6 Microphotographs of cross section and element distribution maps of YSZ | glass #1 | Crofer22APU “sandwich” sealing. The sealing was obtained by heat treatment at 1070 °C for 10 min.

determination of the sealing temperatures, the Crofer22APU interconnector was sealed with YSZ ceramics by each glass at corresponding temperatures. The characterization of the cross sections of the obtained “sandwiches” YSZ | glass | Crofer22APU was carried out by SEM in the SEI and BSE modes to investigate the quality of YSZ/steel connection sealed by the prepared glasses. In addition, this method was used to identify possible chemical interactions between the sealed components. The microphotographs of the samples and the distribution maps of some elements are shown in Figs. 6, 7, 8 and 9. It can be seen that the glass sealants exhibit good adhesion both to YSZ ceramics and to the Crofer22APU stainless steel. According to the distribution maps (Mg, Ca), rare pores are present in the glass phase volume. These pores are likely to have formed due to the combustion of the polymer binder and subsequent gas liberation. The efficiency of removing such gas bubbles depends on the viscosity of the sealing glass, which, in turn, depends on the glass composition and the chosen sealing mode. However, the appeared porosity is of a closed type, thus not causing a depressurization of an electrochemical cell. There is no evidence of chemical interaction between the sealants and YSZ ceramics on the SEM microphotographs. It should be noted that, along with an

increase in the MgO concentration in glass #2, the shape and composition of the phases that form during the sealing of the elements change considerably. Figure 7 depicts needle crystals ($\text{Mg}_3\text{Si}_4\text{O}_{10}$) appearing in glass #2. The main product of crystallization is shown to be sodium silicate (Na_2SiO_3), unlike other tested sealants. In other cases (Figs. 6, 7, 8 and 9), the main product of crystallization is calcium silicate, which is verified by the XRD data (Fig. 2).

Another major problem in creating SOFC assemblies is the formation of chromates due to the interaction of glasses with Cr-containing steels in the oxidative atmosphere [38]. The formation of chromates is known to be an undesirable process, since Cr diffusion into the bulk glass can lead to the failure of a fuel cell. In the study [39], the authors observed the formation of an undesirable chromate layer at the Crofer22APU/glass boundary. The distribution maps of chromium showed the presence of this layer on the glass/interconnector boundary, indicating the interaction of the sealant with the chromium diffused from stainless steel. Under the presence of air, chromates are highly likely to form. It should be mentioned that, in this study, the stability of $\text{SiO}_2\text{-Al}_2\text{O}_3\text{-CaO-Na}_2\text{O-MgO-K}_2\text{O-B}_2\text{O}_3\text{-Y}_2\text{O}_3$ glasses to the Crofer22APU alloy was improved, which is evidenced by the obtained microphotographs and

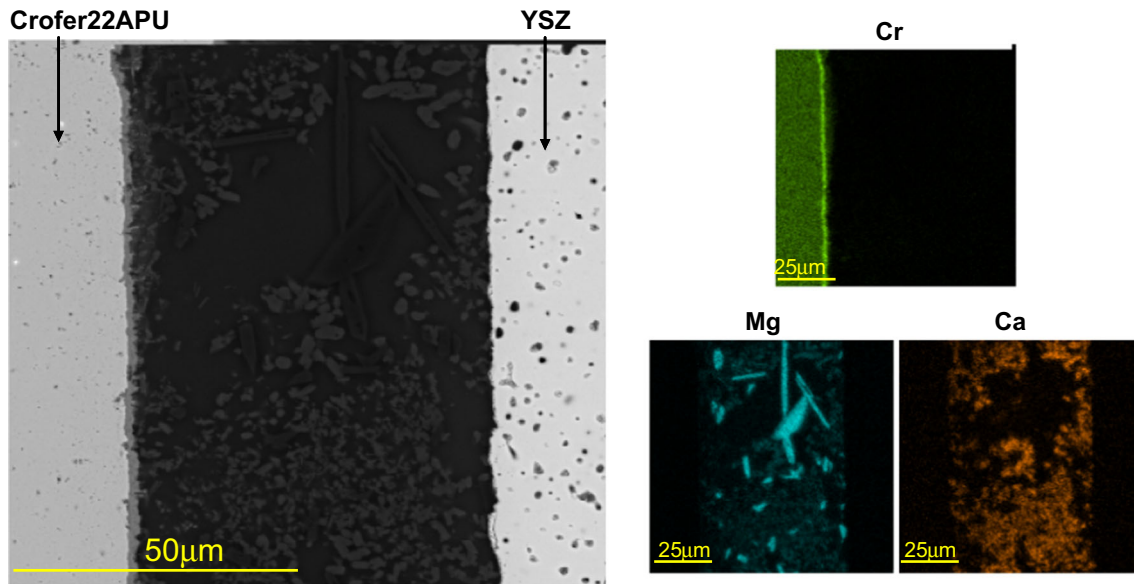


Figure 7 Microphotographs of cross section and element distribution maps of YSZ | glass #2 | Crofer22APU “sandwich” sealing. The sealing was obtained by heat treatment at 1090 °C for 10 min.

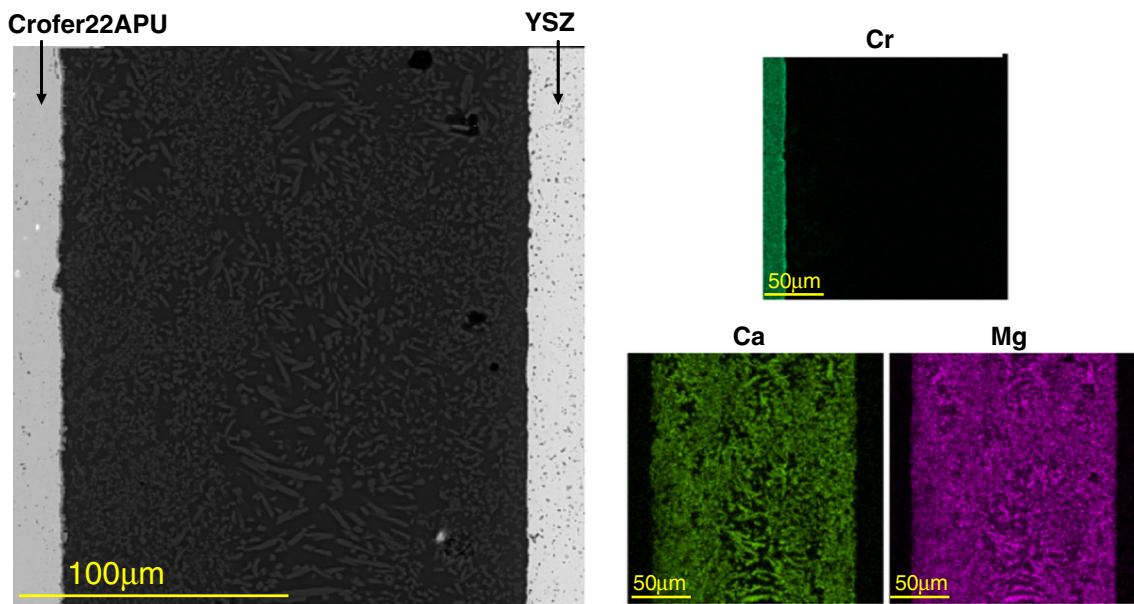


Figure 8 Microphotographs of cross section and element distribution maps of YSZ | glass #3 | Crofer22APU “sandwich” sealing. The sealing was obtained by heat treatment at 1100 °C for 10 min.

element distribution maps. According to Fig. 6, base glass #1 demonstrates a lower stability, interacting with the Crofer22APU alloy with the formation of an irregular wide layer of reaction products at the interface. At the same time, according to Figs. 6 and 7, an increase in MgO concentration and a decrease in Na₂O content allow both the reactivity of the glass to be decreased and a thin homogeneous layer to be

formed on the glass/Crofer22APU boundary, respectively. Hence, Mg-rich glasses seem to be more suitable as glass sealants for SOFC application. For this reason, we tested these glasses for bonding the elements in a tubular single cell.

The scheme of connecting the tubular single elements and the interconnector material in a SOFC is presented in Fig. 10a. Electrolyte-supporting cells

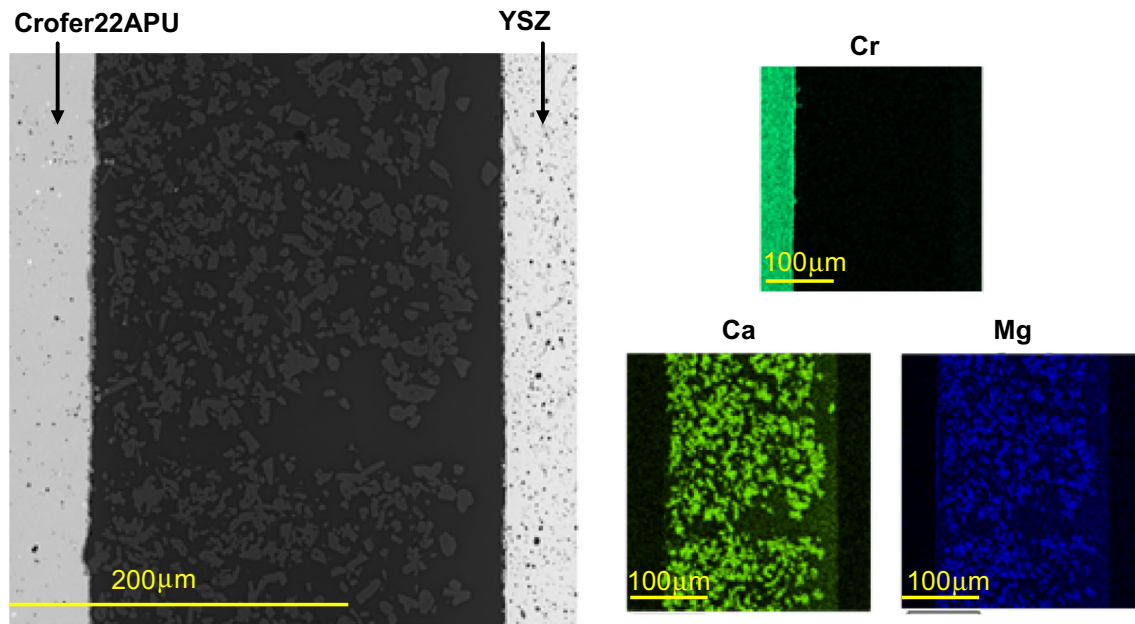


Figure 9 Microphotographs of cross section and element distribution maps of YSZ | glass #6 | Crofer22APU “sandwich” sealing. The sealing was obtained by heat treatment at 1070 °C for 10 min.

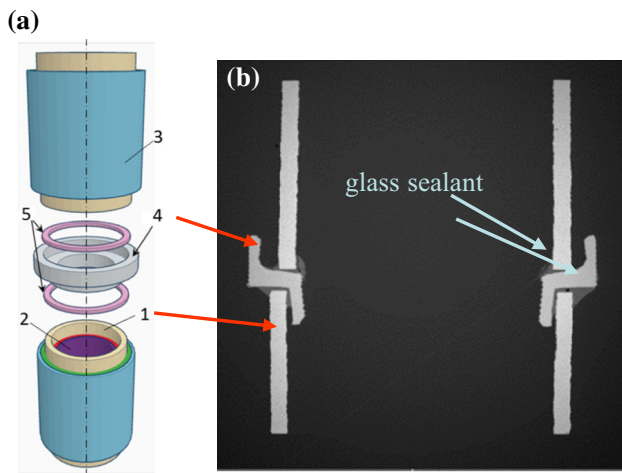


Figure 10 Scheme of SOFC construction **a**, (1—bearing base, 2—cathode, 3—anode, 4—interconnector, 5—glass sealant with a polymeric binder); **b** microphotograph of cross section of two single cells of SOFC with metallic interconnector and glass sealant #2.

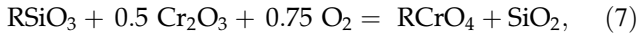
covered with electrode layers are connected by an interconnector, which consists of a stepped ring made of a conductive material. In order to ensure a gas-tight connection between the elements and to prevent the mixing of working gases, a ring made of a high-temperature sealant is secured on the interconnector (on its smaller-diameter side), and another similar ring is inserted into the interconnector (from

its bigger-diameter side). To obtain the ring made of the sealing glass, the glass powder was mixed with an organic binder and a film with a thickness of 0.5 mm was produced. Then, the rings of the certain diameter were cut from this film. The sealing of the single cells was carried out in a vertical furnace with a biasing mechanism at a temperature of 1090 °C for 10 min. In order to provide a reliable electrical contact between the electrode layers and the interconnector, their junctions are coated, respectively, with anode and cathode binders. Figure 10b presents a microphotograph depicting the cross section of two single SOFC cells connected via a Crofer22APU interconnector and sealed with glass #2. It is found that this glass provides a strong connection between tubular SOFC elements during operation at 850 °C for 250 h. Future long-term experiments under SOFC operating conditions should be carried out to determine the degree of the material degradation and to give a quantitative estimation of the crystallization process.

Thermodynamic calculations

The chemical interaction of glass components with chromium can be estimated by the methods of thermodynamics. Since +3 is the most stable oxidation degree for chromium, it should be taken into account

that the surface of a chromium-containing steel is covered by Cr₂O₃. Alkaline and alkaline-earth metals in silicate glasses can be considered as corresponding silicates, thus allowing the following hypothetical interactions to be written:



where R = Na₂, K₂, Mg or Ca. For any temperature above 298.15 K, the enthalpy ($\Delta_r H$) of reaction (7) can be expressed by the equation:

$$\Delta_r H = \sum n_i (\Delta_f H_{298}^\circ)_i + \sum n_i (H^\circ - H_{298}^\circ)_i, \quad (8)$$

where $\Delta_f H_{298}^\circ$ is a standard enthalpy of formation, $H^\circ - H_{298}^\circ$ is an enthalpy increment from 298 K to the desired temperature, i is the index of substance in Eq. (7), and n_i is the corresponding stoichiometric coefficient (positive for the products and negative for the initial reagents). In some handbooks, enthalpy increments are tabulated for different temperatures; otherwise, the increment can be calculated as follows:

$$H^\circ - H_{298}^\circ = \int_{298}^T C_p(T) dt, \quad (9)$$

where $C_p(T)$ is the isobaric heat capacity and T is the absolute temperature. The entropy ($\Delta_r S$) of reaction (7) is equal to:

$$\Delta_r S = \sum n_i S_i, \quad (10)$$

where S_i is the entropy of i -th substance at the desired temperature. The entropy at the desired temperature can be found in handbooks or calculated as:

$$S = S_{298} + \int_{298}^T \frac{C_p(T)}{T} dt, \quad (11)$$

where S_{298} is the entropy at 298 K. Unfortunately, among Na, K, Mg and Ca chromates, the reference literature provides the temperature dependence of heat capacity only for CaCrO₄ [40]. Therefore, we calculated the Gibbs free energy difference ($\Delta_r G$) at 900 K only for R = Ca in reaction (7):

$$\Delta_r G = \Delta_r H - T \Delta_r S. \quad (12)$$

For SiO₂, O₂ and Cr₂O₃, the thermodynamic data were taken from a handbook edited by Glushko [41]. The temperature dependence of the heat capacity of calcium chromate was taken from [40]. The molar heat capacity of CaSiO₃ as a function of temperature was chosen in the form of

$$C_p = 108.5 + 0.018T - 2.463 \times 10^6 T^{-2}, \quad (13)$$

according to Schmetterer and Masset's review [42]. The calculated Gibbs energy difference is equal to -5.3 kJ mol^{-1} ; therefore, reaction (7) for Ca is thermodynamically favourable. Although the information about the temperature dependence of MgCrO₄ heat capacity is lacking, work [43] showed this compound to decompose at temperatures about 600 °C. This implies that magnesium silicate is more thermodynamically preferable at high temperatures compared to magnesium chromate. In contrast, calcium chromate is more stable than its silicate. Hence, magnesium-rich glasses are more resistant to chromate formation.

Conclusion

A number of glass sealants of the Na₂O–K₂O–CaO–MgO–Y₂O₃–Al₂O₃–B₂O₃–SiO₂ system were synthesized. The thermal expansion coefficients (CTEs) of the glasses and glass–ceramics were determined for various compositions. The effect of crystallization on the properties of the sealants was studied. It is found that an increase in B₂O₃ concentration results in a decrease in the glass transition temperature, thus raising the softening temperature of the glass. The CTEs of the synthesized glasses vary across the $9.6\text{--}10.9 \cdot 10^{-6} \text{ K}^{-1}$ range, demonstrating good agreement with those of SOFC materials, i.e. Crofer22APU ($12.1 \cdot 10^{-6} \text{ K}^{-1}$) and YSZ ceramic ($9.4 \cdot 10^{-6} \text{ K}^{-1}$). The crystallization of the glasses is shown to lead to an increase in CTE in all the cases.

SEM characterization has shown the synthesized glasses to form a gas-tight sealing between YSZ/glass/Crofer22APU with their good adhesion to the materials to be glued. The sealing temperatures of the obtained samples vary across the 1070–1100 °C range, which values are lower than the maximum permissible operating temperature of the Crofer22-APU alloy. No chemical interaction was observed at the electrolyte/glass interface. However, at the Crofer22APU/glass boundary, a thin layer of products resulting from the interaction of the glass components with chromium was formed. The experimental data and thermodynamic calculations have shown that the intensity of interaction between Cr-containing steel and the glass sealants can be reduced by

increasing the magnesium oxide concentration and decreasing the calcium oxide concentration. In this respect, composition #2 is found to be more suitable for SOFC application. Glass #2 has been tested as a sealant for a tubular SOFC. The stability of the connection between the SOFC constituting components was verified during operation at 850 °C for 250 h. It can be concluded that the results of this work can be applied to industry scale fabrication of tubular solid oxide fuel cells.

Acknowledgements

This study was financially supported by the RFBR-BRFFR project (RFBR Grant No. 17-58-04116, BRFFR Grant No. X17PM-033). The research was partially performed using the facilities of the Shared Access Centre “Composition of Compounds” of IHTe UB RAS. The authors thank S.V. Plaksin, E.A. Sherstobitova and V.A. Eremin for their assistance in conducting the research.

References

- [1] Höland W, Beall G (2012) Glass-ceramic technology. Wiley, Hoboken
- [2] Smeacetto F, Miranda A, Chrysanthou A et al (2014) Novel glass-ceramic composition as sealant for SOFCs. *J Am Ceram Soc* 97:3835–3842
- [3] Gurbinder K (2016) Solid oxide fuel cell components. Springer International Publishing, Switzerland
- [4] Mahato N, Banerjee A, Gupta A et al (2015) Progress in material selection for solid oxide fuel cell technology: a review. *Prog Mater Sci* 72:141–337
- [5] Lessing PA (2007) A review of sealing technologies applicable to solid oxide electrolysis cells. *J Mater Sci* 42:3465–3476. <https://doi.org/10.1007/s10853-006-0409-9>
- [6] Maharapta MK, Lu K (2010) Glass-based seals for solid oxide fuel and electrolyzer cells—a review. *Mater Sci Eng, R* 67:65–85
- [7] Ley KL, Krumplet M, Kumar R et al (1996) Glass-ceramic sealants for solid oxide fuel cells: part I. Physical properties. *J Mater Res* 11:1489–1493
- [8] Eichler K, Solow G, Otschik P et al (1999) BAS (BaO·Al₂O₃·SiO₂)-glasses for high temperature applications. *J Eur Ceram Soc* 19:1101–1104
- [9] Sohn SB, Choi SY (2004) Suitable glass-ceramic sealant for planar solid-oxide fuel cells. *J Am Ceram Soc* 87:254–260
- [10] Larsen PH, James PF (1998) Chemical stability of MgO/CaO/Cr₂O₃–Al₂O₃–B₂O₃–phosphate glasses in solid oxide fuel cell environment. *J Mater Sci* 33:2499–2507. <https://doi.org/10.1023/A:1004332614379>
- [11] Nielsen KA, Solvang M, Nielsen SBL et al (2007) Glass composite seals for SOFC application. *J Eur Ceram Soc* 27:1817–1822
- [12] Chou YS, Stewenson JW, Choi JP (2013) Evaluation of a single cell and candidate materials with high water content hydrogen in a generic solid oxide fuel cell stack test fixture, part II: materials and interface characterization. *Int J Appl Ceram Technol* 10:97–106
- [13] Donald IW, Mallison PM, Metcalfe BL et al (2011) Recent developments in the preparation, characterization and applications of glass- and glass-ceramic-to-metal seals and coatings. *J Mater Sci* 46:1975–2000. <https://doi.org/10.1007/s10853-010-5095-y>
- [14] Reddy AA, Tulyaganov DU, Pascual MJ et al (2013) Diopside–Ba disilicate glass–ceramic sealants for SOFCs: enhanced adhesion and thermal stability by Sr for Ca substitution. *Int J Hydrogen Energy* 38:3073–3086
- [15] Smeacetto F, Salvo M, Ferraris M, Casalegno V, Asinari P, Chrysanthou A (2008) Characterization and performance of glass–ceramic sealant to join metallic interconnects to YSZ and anode-supported-electrolyte in planar SOFCs. *J Eur Chem Soc* 28:2521–2527
- [16] Smeacetto F, Salvo M, Ferraris M, Casalegno V, Asinari P (2008) Glass and composite seals for the joining of YSZ to metallic interconnect in solid oxide fuel cells. *J Eur Chem Soc* 28:611–616
- [17] Smeacetto F, Salvo M, Ferraris M, Cho J, Boccaccini AR (2008) Glass–ceramic seal to join Crofer 22 APU alloy to YSZ ceramic in planar SOFCs. *J Eur Chem Soc* 28:61–68
- [18] Smeacetto F, Chrysanthou A, Salvo M, Zhang Z, Ferraris M (2009) Performance and testing of glass-ceramic sealant used to join anode-supported-electrolyte to Crofer22APU in planar solid oxide fuel cells. *J Power Sources* 190:402–407
- [19] Smeacetto F, Chrysanthou A, Salvo M et al (2011) Thermal cycling and ageing of a glass-ceramic sealant for planar SOFCs. *Int J Hydrogen Energy* 36:11895–11903
- [20] Smeacetto F, Salvo M, Leone P et al (2011) Performance and testing of joined Crofer22APU-glass-ceramic sealant-anode supported cell in SOFC relevant conditions. *Mater Lett* 65:1048–1052
- [21] Smeacetto F, Salvo M, Santarelli M, Leone P et al (2013) Performance of a glass-ceramic sealant in a SOFC short stack. *Int J Hydrogen Energy* 38:588–596
- [22] Smeacetto F, Chrysanthou A, Moskalewicz T, Salvo M (2013) Thermal cycling of Crofer22APU-sealant-anode

- supported electrolyte joined structures for planar SOFCs up to 3000 h. *Mater Lett* 111:143–146
- [23] Smeacetto F, Radaelli M, Salvo M et al (2017) Glass-ceramic joining material for sodium-based battery. *J Ceram Int* 43:8329–8333
- [24] Smeacetto F, Miranda A, Polo SC et al (2015) Electrophoretic deposition of Mn_{1.5}Co_{1.5}O₄ on metallic interconnect and interaction with glass-ceramic sealant for solid oxide fuel cells application. *J Power Sources* 280:379–386
- [25] Smeacetto F, De Miranda A, Ventrella A, Salvo M, Ferraris M (2015) Shear strength tests of glass ceramic sealant for solid oxide fuel cells applications. *Adv Appl Ceram* 114:70–75
- [26] Smeacetto F, Salvo M, D'Hérin Bytner FD, Leone P, Ferraris M (2010) New glass and glass-ceramic sealants for planar solid oxide fuel cells. *J Eur Chem Soc* 30:933–940
- [27] Sabato AG, Cempura G, Montinaro D, Chrysanthou A, Salvo M, Bernardo E, Secco M, Smeacetto F (2016) Glass-ceramic sealant for solid oxide fuel cells application: characterization and performance in dual atmosphere. *J Power Sources* 328:262–270
- [28] Sabato AG, Salvo M, De Miranda A, Smeacetto F (2015) Crystallization behaviour of glass-ceramic sealant for solid oxide fuel cells. *Mater Lett* 141:284–287
- [29] Krainova DA, Zharkina ST, Saetova NS et al (2017) Influence of cerium oxide on properties of glass-ceramic sealants for solid oxide fuel cells. *Rus J Appl Chem* 90:1047–1053
- [30] Gropp S, Fischer M, Dittrich L et al (2015) Wetting behaviour of glasses on nanostructured silicon surfaces. *J Electr Eng* 3:15–20
- [31] Borhan AI, Gromada M, Nedelcu GG, Leontie L (2016) Influence of (CoO, CaO, B₂O₃) additives on thermal and dielectric properties of BaO–Al₂O₃–SiO₂ glass ceramic sealant for OTM applications. *J Ceram Int* 42:10459–10468
- [32] Pershina SV, Raskovalov AA, Antonov BD et al (2015) Extreme behavior of Li-ion conductivity in the Li₂O–Al₂O₃–P₂O₅ glass system. *J Non-Cryst Solids* 430:64–72
- [33] Nechaev GV, Vlasova SG, Reznitskikh OG (2015) Conductivity in sodium-yttrium-silicate and sodium-yttrium-phosphate glass. *Glass Phys Chem* 41:64–67
- [34] Lasocka M (1976) The effect of scanning rate on glass transition temperature of splat-cooled Te₈₅Ge₁₅. *J Mater Sci Eng* 23:173–177
- [35] Ota T, Matsubara T, Takahashi M et al (1995) Thermal expansion of nepheline–leucite ceramic composites. *J Ceram Soc Jpn* 103:523–524
- [36] Appen AA (1974) Himiya stekla. Himia, Leningrad
- [37] Fluegel Alexander (2010) Thermal expansion calculation for silicate glasses at 210°C based on a systematic analysis of global databases. *Glass Technol-Part A* 51:191–201
- [38] Chou Y, Stevenson JW, Singh P (2008) Effect of aluminizing of Cr-containing ferritic alloys on the seal strength of a novel high-temperature solid oxide fuel cell sealing glass. *J Power Sources* 185:1001–1008
- [39] Reis ST, Pascual MJ, Brow RK et al (2010) Crystallization and processing of SOFC sealing glasses. *J Non-Cryst Solids* 356:3009–3012
- [40] Lee YM, Nassaralla CL (2001) Heat capacities of calcium chromate and calcium chromite. *Thermochim Acta* 371:1–5
- [41] Glushko VP, Gurvich LV, Bergman GA, Veits IV, Medvedev VA, Khachkuruzov GA, Yungman VS (1978–1982) Thermodynamic properties of individual materials, Nauka, Moskva (Russia), V. I–IV
- [42] Schmetterer C, Masset PJ (2012) Heat capacity of compounds in the CaO–SiO₂ system—a review. *J Phase Equilibria Diffusion* 33:261–275
- [43] Nisino T, Moteki K, Sikano H (1963) Thermal decomposition of magnesium chromate. *J Ceram Assoc* 71:159–163